Methane Decomposition into Hydrogen and Carbon Nanofibers over Supported Pd−Ni Catalysts: Characterization of the Catalysts during the Reaction

Sakae Takenaka,*,† Yukio Shigeta,† Eishi Tanabe,‡ and Kiyoshi Otsuka*,†

Department of Applied Chemistry, Graduate School of Science and Engineering, Tokyo Institute of Technology, Ookayama, Meguro-ku, Tokyo 152-8552, Japan, and Western Hiroshima Prefecture Industrial Institute, Kagamiyama, Higashi-Hiroshima, Hiroshima 739-0046, Japan

Received: December 6, 2003; In Final Form: April 2, 2004

The addition of Pd into Ni/SiO_2 improved the catalytic activity and life for methane decomposition into hydrogen and carbon nanofibers. Thus, Pd-added Ni/SiO_2 (denoted as $Pd-Ni/SiO_2$) was characterized by measuring the Ni and Pd K-edge XANES and EXAFS and TEM images. Methane decomposition on Ni/SiO_2 or Pd/SiO_2 formed carbon nanofibers with Ni or Pd metal particles at the tips of them. Ni metal in Ni/SiO_2 was transformed into Ni carbides at the deactivation stage of the catalyst for methane decomposition. Pd metal particles in Pd/SiO_2 were fragmented into smaller ones during methane decomposition. On the other hand, $Pd-Ni/SiO_2$ produced carbon nanofibers of different shapes than those on Ni/SiO_2 and Pd/SiO_2, i.e., branched carbon nanofibers. The local structure and average crystallite size of Pd−Ni alloys in $Pd-Ni/SiO_2$ did not change appreciably during methane decomposition, but the shape of alloy particles changed gradually. The number of facets on Pd−Ni alloy particles that precipitated carbon atoms increased during methane decomposition. This explains the increase in the catalytic life as well as the formation of branched carbon nanofibers.

Introduction

Methane decomposition ($CH_4 \rightarrow C + 2H_2$) is of current interest from a viewpoint of the synthesis of pure hydrogen and carbon nanofibers.[1−3] It is well-known that supported Ni catalysts were one of the promising catalysts for methane decomposition.[4−7] We have also reported that silica-supported Ni catalyst (Ni/SiO_2) showed a high activity for methane decomposition in the temperature range of 773−873 K.[8] Supported Ni catalysts produce carbon nanofibers with a Ni metal particle at the tip of them. A well-accepted mechanism for methane decomposition by Ni metal includes the activation of methane on Ni metal particles and the formation of surface carbons, followed by carbon diffusion across the Ni metal particles and growth of carbon nanofibers.[4,9] However, the catalytic life of supported Ni catalysts for methane decomposition was relatively short, especially at reaction temperatures >873 K. It is desirable that methane decomposition is performed at >873 K, because one-pass conversions of methane are restricted to low levels by thermodynamic equilibrium at lower temperatures. Thus, a catalyst with higher activity and longer life for the reaction at >873 K is required in order to attain higher conversions of methane.

Some reports indicated that catalysts made of bimetallic particles were superior compared with those made of monometallic ones, in terms of activity, selectivity, and stability.[10,11] As for methane decomposition, the addition of foreign metals into supported-Ni catalysts improved the catalytic activity and life, depending on the kinds of the additives.[12−14] In addition, the modification with foreign metals could influence the mechanism of growth of carbon nanofibers described above. For example, the addition of Cu into Ni-based catalysts enhanced the catalytic activity and life for the methane decomposition.[15−19] It was proposed that the formation of Cu−Ni alloys brought about an improvement of the catalytic performance for the reaction. In addition, Ni catalysts modified with Cu (denoted as Cu−Ni catalysts hereafter) produced carbon nanofibers with a different structure from that formed by the catalyst without this additive. The structures of metal components in Cu−Ni catalysts were investigated to elucidate the effect of Cu addition on the catalytic performance. However, little attention focused on the structural changes of catalytically active metal components in the catalysts during methane decomposition. We have recently reported that Pd addition into supported Ni catalysts improved the catalytic performance for methane decomposition, especially the catalytic life.[20,21] The catalysts modified with Pd (denoted as Pd−Ni catalysts hereafter) showed higher activity and longer life for methane decomposition, even in the temperature range from 873 to 1073 K, while Ni catalyst without Pd was deactivated quickly for the reaction at >873 K. In addition, Pd−Ni catalysts produced carbon nanofibers of different shapes from those formed by Ni catalysts without this additive. We believe that the structural changes of catalytically active metal components during methane decomposition should be examined in order to elucidate synergy effects between these metals on the catalytic performance for the reaction.

The changes of the local structures and shapes of catalytically active metal components in $Ni-Pd/SiO_2$, Ni/SiO_2, and Pd/SiO_2 during methane decomposition were examined by measuring Ni and Pd K-edge XANES and EXAFS and also TEM images in the present study. On the basis of these results, the effects of Pd addition into Ni catalysts on the catalytic performance for methane decomposition were discussed.

* Corresponding author. Tel.: 81-3-5734-2626. Fax: 81-3-5734-2879. E-mail: stakenak@o.cc.titech.ac.jp.
† Tokyo Institute of Technology.
‡ Western Hiroshima Prefecture Industrial Institute.

10.1021/jp0377331 CCC: $27.50
Published on Web 05/07/2004

Experimental Section

Ni/SiO_2, Pd/SiO_2, and $Pd-Ni/SiO_2$ were prepared by a conventional impregnation method. $Ni(NO_3)_2 \cdot 6H_2O$ and $PdCl_2$ were used as metal sources for the preparation of the catalysts. Cab-O-Sil (Cabot Co., specific surface area = 200 $m^2\ g^{-1}$) was used as a silica support. Silica support was impregnated with an aqueous solution containing metal cations (Ni and/or Pd) at 363 K. The impregnated samples were dried at 373 K for 10 h.

Methane decomposition was carried out with a conventional gas-flow system. The catalyst was packed in a tubular reactor (diameter = 2 cm and length = 60 cm) made from quartz. Prior to the reaction, the catalyst was reduced by hydrogen at 573 K for 1 h and treated with Ar at 923 K for 6 h. After the pretreatment of the catalyst, methane was reacted with the catalyst at the required temperature. During methane decomposition, a part of gases at the exit of the catalyst bed was sampled and analyzed by GC.

X-ray diffraction (XRD) patterns of the catalyst samples were measured by a Rigaku RINT 2500V diffractometer using Cu Kα radiation at room temperature.

SEM and TEM images of carbons deposited on the catalysts by methane decomposition were measured using a Hitachi FE-SEM S-800 (field emission gun scanning electron microscope) and a JEOL JEM-3000F, respectively.

X-ray absorption spectra (XANES and EXAFS) were measured on the beam line BL-7C for Ni K-edge absorption and on the beam line BL-10B for Pd K-edge absorption at Photon Factory in the Institute of Materials Structure Science for High Energy Accelerator Research Organization at Tsukuba in Japan (Proposal Number 2002G255). Ni K-edge XANES and EXAFS of the catalyst samples were measured in fluorescence mode with a Si(111) two-crystal monochromator at room temperature. Pd K-edge XANES and EXAFS of the catalyst samples were recorded in transmission mode with a Si(311) channel-cut monochromator at room temperature. To prepare the catalyst samples for the measurements of XANES and EXAFS, the catalyst samples that had been reduced with hydrogen at 573 K and subsequently treated with Ar at 923 K were contacted with methane at 873 K for the required time. After the reaction, the catalyst samples were cooled to room temperature under an Ar stream. Then, each catalyst was packed in a bag made from polyethylene under argon atmosphere. The analysis of EXAFS data was performed by using an EXAFS analysis program, REX (Rigaku Co.). For EXAFS analysis, the oscillation was extracted from the EXAFS data by a spline smoothing method. The oscillation was normalized by the edge height around 70−100 eV above the threshold. The Fourier transformation of k^3-weighted EXAFS oscillation was performed over the range of $k = 3.5-15.5$ $Å^{-1}$. Inversely Fourier transformed data for each Fourier peak were analyzed by a curve-fitting method, using theoretically phase-shift and amplitude functions derived by the program FEFF8.[22]

Results and Discussion

Catalytic Performance of $Pd-Ni/SiO_2$ for Methane Decomposition. Figure 1 shows the change of methane conversion with time on a stream of methane for methane decomposition over Ni/SiO_2, Pd/SiO_2, and $Pd-Ni/SiO_2$ catalysts at 923 K. The loading of metals (Pd and Ni) in all the catalysts was adjusted to be 10 mol %. $Pd-Ni/SiO_2$ catalysts of mole ratio Pd/(Pd + Ni) = 0.25, 0.50, and 0.75 were tested for methane decomposition. Methane decomposition proceeded selectively over all the catalysts to form hydrogen as a gaseous product. Pd/SiO_2 and Ni/SiO_2 showed the catalytic activity for methane decomposition at the early stage of the reaction. However, methane conversions for these catalysts were declined quickly, and finally, these catalysts were deactivated completely within 2 h. The catalytic activity and life of $Pd-Ni/SiO_2$ were extremely superior to those of Pd/SiO_2 and Ni/SiO_2. Methane conversion during the early stage and catalytic life for $Pd-Ni/SiO_2$ were strongly dependent on the mole ratio Pd/(Pd + Ni). Hydrogen yields [H_2/(Pd + Ni); moles of hydrogen formed per 1 mol of metals in the catalysts] until the complete deactivation of the catalysts were estimated by integrating the formation rate of hydrogen against time on stream in Figure 1, assuming that methane decomposition into hydrogen and carbon proceeded selectively. The hydrogen yields were evaluated to be 410 for Ni/SiO_2, 480 for Pd/SiO_2, and 11 300, 16 330, and 6490 for the catalysts of Pd/(Pd + Ni) ratio 0.25, 0.50, and 0.75, respectively. These results indicated that coexistence of Pd and Ni in the catalyst enhanced the catalytic life and hydrogen yield for methane decomposition. The $Pd-Ni/SiO_2$ of Pd/(Pd + Ni) = 0.5 showed the highest hydrogen yield among all the catalysts tested in the present work.

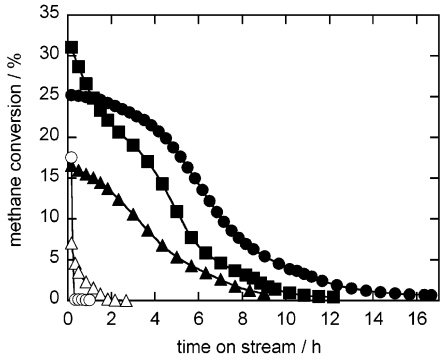

Figure 1. Change of methane conversion with time on a stream of methane over Ni/SiO_2, Pd/SiO_2, and $Pd-Ni/SiO_2$ catalysts at 923 K. Catalysts = 0.02 g, methane = 60 mL min^{-1}, and 101 kPa. Loading of metal (Pd and/or Ni) for all the catalysts = 10 mol %. Pd/(Pd + Ni) mole ratio: ○, 0 (Ni/SiO_2); ■, 0.25; ●, 0.50; ▲, 0.75; △, 1.0 (Pd/SiO_2).

Figure 2 shows SEM and TEM images of carbons deposited on Ni/SiO_2, Pd/SiO_2, and $Pd-Ni/SiO_2$ catalysts by methane decomposition. SEM image a shows the preferential formation of carbon nanofibers by methane decomposition over Ni/SiO_2. The diameters of carbon nanofibers on Ni/SiO_2 were relatively uniform (60−100 nm). Pd/SiO_2 also grew carbon nanofibers by methane decomposition (SEM image b), although the diameters of carbon nanofibers were too small to observe the shape of them clearly from the image. The diameters of carbon nanofibers on Pd/SiO_2 were distributed widely from 10 to 150 nm. On the other hand, the shape of carbons deposited on $Pd-Ni/SiO_2$ was different from those on Ni/SiO_2 and Pd/SiO_2. From SEM image c, carbon nanofibers of a variety of diameters from 30 to 300 nm could be seen. The most characteristic point for $Pd-Ni/SiO_2$ is the formation of branched carbon nanofibers, as shown in SEM image e and TEM image f, in addition to carbon nanofibers that were observed on Ni/SiO_2 and Pd/SiO_2. Carbon nanofibers with branched structures could not be seen in SEM or TEM images for Ni/SiO_2 or Pd/SiO_2. Besides branched fibers, coarse fibers were formed on $Pd-Ni/SiO_2$, as found in the SEM image d. These results indicated that the mechanism of carbon deposition on $Pd-Ni/SiO_2$ is significantly different from that on Ni/SiO_2 and Pd/SiO_2.

Characterization of the Catalysts. We investigated the structures of catalytically active metal components in Pd/SiO_2, Ni/SiO_2, and $Pd-Ni/SiO_2$ by measuring Ni K-edge and Pd K-edge XANES/EXAFS and by XRD analysis. The shapes of metal components and carbons deposited from methane on these

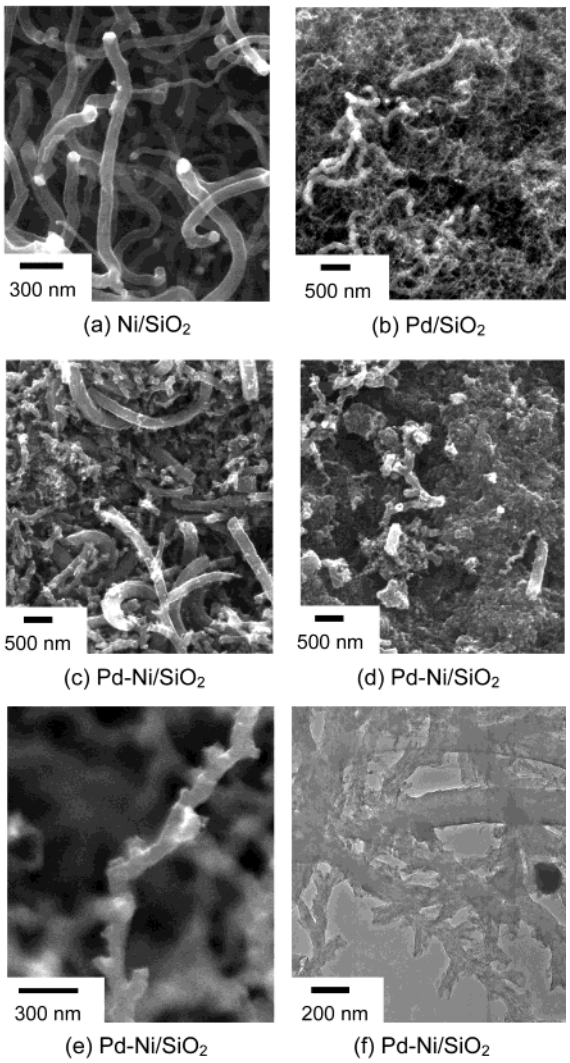

Figure 2. SEM and TEM images of carbon nanofibers deposited on Ni/SiO_2 (a), Pd/SiO_2 (b), and $Pd-Ni/SiO_2$ (c−f). Metal loading for all the catalysts = 10 mol %, mole ratio Pd/(Pd + Ni) = 0.5. (a−e) SEM images, (f) TEM image.

catalysts were examined by TEM images. $Pd-Ni/SiO_2$ of mole ratio Pd/(Pd + Ni) = 0.5 was utilized for the spectroscopic measurements, because this mole ratio was the optimum value for methane decomposition, as described above. Measurements of XANES/EXAFS, XRD patterns and TEM images for the catalysts were performed before and after methane decomposition in order to clarify the structural change of catalytically active metal components during the reaction. Methane decomposition was compulsorily terminated while the catalysts were still active for the reaction, i.e., C/Ni = 50 and 650 for Ni/SiO_2, C/Pd = 7 and 118 for Pd/SiO_2, and C/(Pd + Ni) = 7, 310, and 860 for $Pd-Ni/SiO_2$ [C/Ni, C/Pd, and C/(Pd + Ni); moles of carbons deposited per mole of metals (Pd and Ni) in the catalysts]. In addition, the structures of metal components for these catalysts after the complete deactivation for methane decomposition were also examined, i.e., Ni/SiO_2 with deposited carbons of C/Ni = 1100, Pd/SiO_2 with C/Pd = 260, and $Pd-Ni/SiO_2$ with C/(Pd + Ni) = 2360. Methane decomposition for $Pd-Ni/SiO_2$ and Pd/SiO_2 was performed at 873 K. The reaction for Ni/SiO_2 was performed at 803 K, because the life of this catalyst was too short at 873 K to adjust the amount of carbons deposited on the catalyst.[8] Because carbon yield for $Pd-Ni/SiO_2$ of mole ratio Pd/(Pd + Ni) = 0.5 until the complete deactivation was too large under the reaction conditions in Figure 1, the loading of (Pd + Ni) decreased from 13.5 to 10 wt % and the reaction temperature decreased from 923 to 873 K for the spectroscopic measurements. When too much carbon was deposited on the catalyst, it was difficult to obtain the spectra with a high signal-to-noise ratio due to the dilution of metal components by deposited carbons.

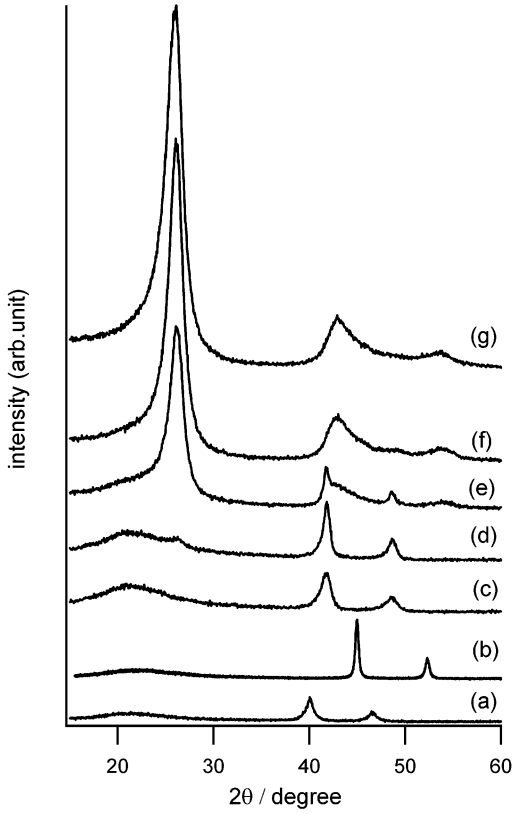

Figure 3. XRD patterns of Ni/SiO_2, Pd/SiO_2, and $Pd-Ni/SiO_2$: (a) fresh Pd/SiO_2; (b) fresh Ni/SiO_2; (c, d, e, f, and g) $Pd-Ni/SiO_2$ with deposited carbons of C/(Pd + Ni) = 0 (fresh), 7, 310, 860, and 2360, respectively. Metal loading for all the catalysts = 10 wt %.

Structure of Catalytically Active Metal Components in the Catalysts. Figure 3 shows XRD patterns of Ni/SiO_2, Pd/SiO_2, and $Pd-Ni/SiO_2$ catalysts. Diffraction peaks due to Pd metal at $2\theta = 40.0°$ and 46.5° for fresh Pd/SiO_2 (spectrum a) and those due to Ni metal at $2\theta = 44.8°$ and 52.5° for fresh Ni/SiO_2 (spectrum b) were observed, suggesting that most of metal species in Pd/SiO_2 and Ni/SiO_2 were present as a crystallized Pd and Ni metal, respectively. On the other hand, peaks appeared at $2\theta = 41.8°$ and 48.5° for the XRD pattern of fresh $Pd-Ni/SiO_2$ (spectrum c), indicating that Pd−Ni alloys were formed in the catalyst. The peaks due to Pd−Ni alloys for the catalysts with deposited carbons of C/(Pd + Ni) = 7 and 310 (spectra d and e) were observed at the same positions as those of the fresh catalyst. Thus, the fraction of each component (Pd and Ni) in Pd−Ni alloys did not change during methane decomposition in the range of C/(Pd + Ni) = 0−310. However, the peaks due to Pd−Ni alloys disappeared in the range of C/(Pd + Ni) ≥ 860 (spectra f and g). This would result from the dilution of metal species by deposited carbons. New peaks due to deposited carbons appeared at $2\theta = 26.0$, 43.0° and 53.5° in the XRD patterns of $Pd-Ni/SiO_2$ after methane decomposition (spectra d−g). These peaks became stronger with an increase in the amount of deposited carbons.

Figure 4 shows Ni K-edge XANES spectra of Ni/SiO_2 and $Pd-Ni/SiO_2$ catalysts, before and after methane decomposition, and of Ni foil. XANES spectra of fresh Ni/SiO_2 catalyst

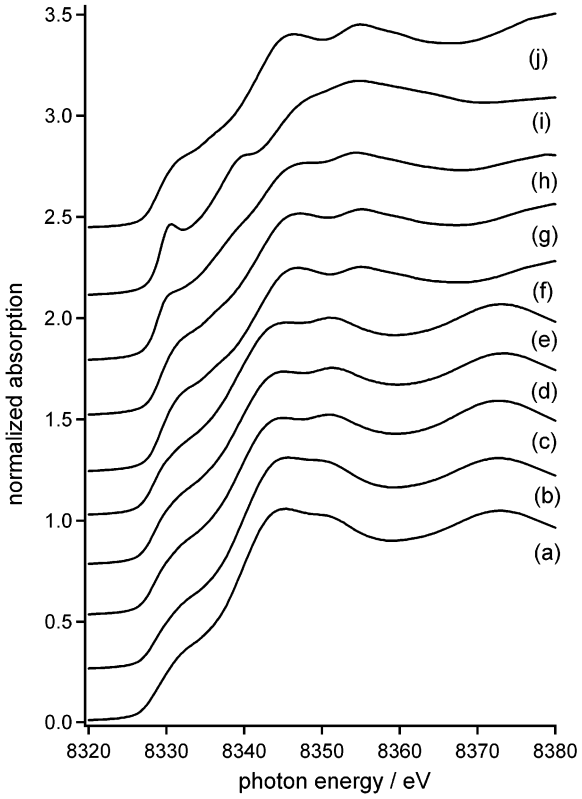

Figure 4. Ni K-edge XANES spectra of Ni/SiO_2, $Pd-Ni/SiO_2$, and Ni foil: (a, b, c, d, and e) $Pd-Ni/SiO_2$ with deposited carbons of C/(Pd + Ni) = 0 (fresh), 7, 310, 860 and 2360, respectively; (f, g, h, and i) Ni/SiO_2 with deposited carbons of C/Ni = 0 (fresh), 50, 650 and 1100, respectively; (j) Ni foil. Loading of (Pd + Ni) for $Pd-Ni/SiO_2$ = 10 wt %. Loading of Ni for Ni/SiO_2 = 5 wt %.

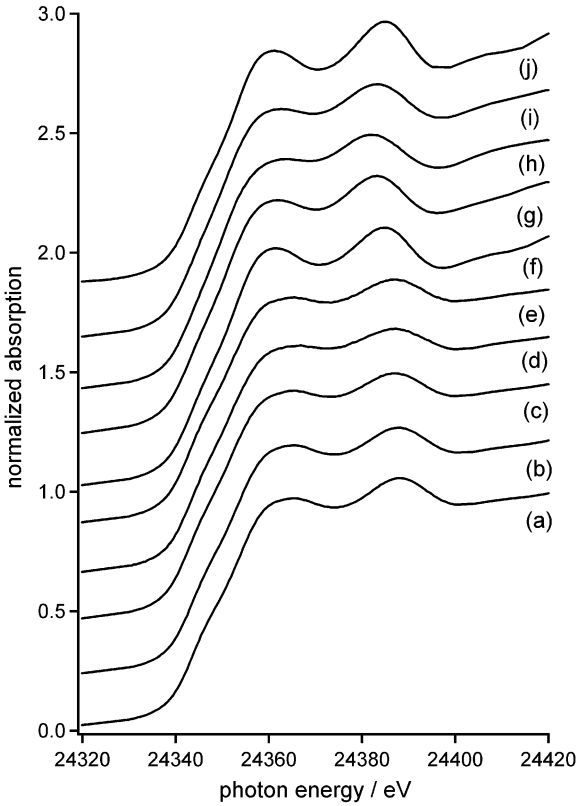

Figure 5. Pd K-edge XANES spectra of Pd/SiO_2, $Pd-Ni/SiO_2$, and Pd foil: (a, b, c, d, and e) $Pd-Ni/SiO_2$ with deposited carbons of C/(Pd + Ni) = 0 (fresh), 7, 310, 860, and 2360, respectively; (f, g, h, and i) Pd/SiO_2 with deposited carbons of C/Pd = 0 (fresh), 7, 118, and 260, respectively; (j) Pd foil. Loading of (Pd + Ni) for $Pd-Ni/SiO_2$ = 10 wt %. Loading of Pd for Pd/SiO_2 = 10 wt %.

(spectrum f) and of the catalysts with deposited carbons of C/Ni = 50 and 650 (spectra g and h) were compatible with that of Ni foil (spectrum j), indicating that Ni species were present as Ni metal when the catalyst was active for the reaction. However, new peaks appeared at around 8330 and 8340 eV for XANES (spectrum i) of the deactivated Ni/SiO_2. In addition, two peaks at 8345 and 8355 eV, which were observed in the spectrum of Ni foil, became weak for the spectrum of the deactivated catalyst. These spectral changes can be ascribed to the formation of Ni carbides at the deactivation stage.[23]

XANES spectrum of fresh $Pd-Ni/SiO_2$ (spectrum a) was different from that of Ni foil. The XRD pattern of fresh $Pd-Ni/SiO_2$ in Figure 3 suggested the formation of Pd−Ni alloys. Thus, the XANES spectrum of fresh $Pd-Ni/SiO_2$ could be assignable to Pd−Ni alloys. A peak at 8343 eV in the XANES spectrum of the fresh catalyst became slightly weak when it was contacted with methane. The absorption at 8343 eV became stronger when Ni species were oxidized.[24] Therefore, the spectral change at the early stage of methane decomposition could be ascribed to the reduction of a part of Ni species in Pd−Ni alloys with methane. Pd−Ni alloy particles in $Pd-Ni/SiO_2$ interacted with SiO_2 support before contact of methane. Ni species in the alloy that are contacted directly with SiO_2 support may be slightly oxidized due to the formation of Ni−O−Si bonds. By contact of methane with the fresh catalyst, alloy particles decomposed methane and precipitated carbon atoms to form carbon nanofibers. Therefore, the alloy particles did not contact with SiO_2 but with carbons directly after contact of methane with the catalyst. This would bring about the reduction of Ni species in the alloys. On the other hand, XANES spectra of $Pd-Ni/SiO_2$ did not change appreciably in the range of C/(Pd + Ni) ≥ 310 (spectra c−e), while XANES spectra of Ni/SiO_2 changed at the deactivation stage. The XANES spectra of $Pd-Ni/SiO_2$ were similar to those of Pd−Ni nanoclusters.[25] These results suggest that the local structure of Pd−Ni alloys in $Pd-Ni/SiO_2$ did not change significantly during methane decomposition.

Figure 5 shows Pd K-edge XANES spectra of Pd/SiO_2 and $Pd-Ni/SiO_2$, before and after methane decomposition, and of Pd foil. The XANES spectrum of fresh Pd/SiO_2 (spectrum f) was consistent with that of Pd foil (spectrum j), suggesting that Pd species in the fresh catalyst were present as Pd metal. Contact of methane with Pd/SiO_2 caused the change of XANES spectra, i.e., the peak at 24385 eV for the fresh catalyst was shifted to 24383 eV (spectra g−i). McCaulley reported the similar change of XANES spectra to that in the present study, when Pd metal was transformed into Pd carbides.[26] In addition, the EXAFS spectra of Pd/SiO_2 suggested the formation of Pd carbide species during methane decomposition, as will be described later. Thus, the change of Pd K-edge XANES of Pd/SiO_2 after contact of methane can be ascribed to the formation of Pd carbide species.

The Pd K-edge XANES spectrum of fresh $Pd-Ni/SiO_2$ (spectrum a) was different than that of Pd foil, i.e., the positions of two peaks observed in the range from 24360 to 24390 eV in the spectra of $Pd-Ni/SiO_2$ were not consistent with those for Pd foil. This can be ascribed to the formation of Pd−Ni alloys in $Pd-Ni/SiO_2$ catalyst. XANES spectra of all the $Pd-Ni/SiO_2$ (spectra b−e) were similar to one another irrespective of different amounts of deposited carbons from 7 to 2360, suggesting that the local structure around Pd atoms in Pd−Ni alloys did not change appreciably during methane decomposition over $Pd-Ni/SiO_2$.

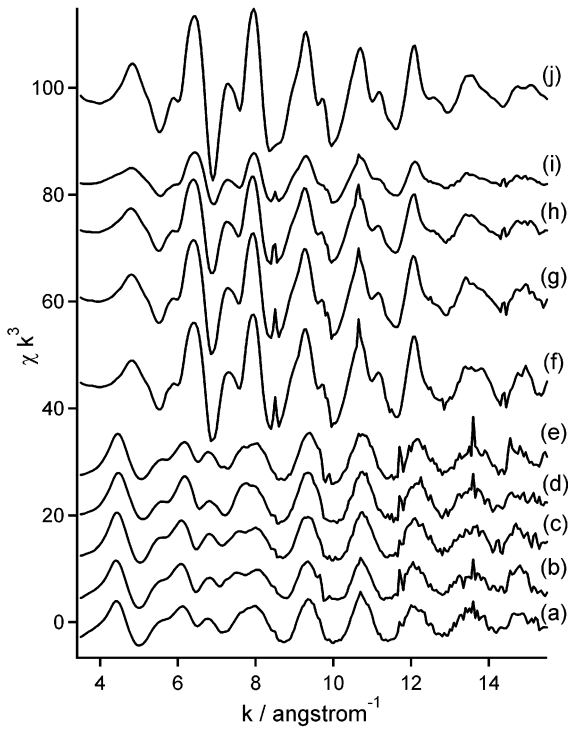

Figure 6. Ni K-edge k^3-weighted EXAFS of Pd−Ni/SiO_2, Ni/SiO_2, and Ni foil: (a, b, c, d, and e) Pd−Ni/SiO_2 with deposited carbons of C/(Pd + Ni) = 0 (fresh), 7, 310, 860, and 2360, respectively; (f, g, h, and i) Ni/SiO_2 with deposited carbons of C/Ni = 0 (fresh), 50, 650, and 1100, respectively; (j) Ni foil. Intensity of χk^3 for a Ni foil was decreased to one-third.

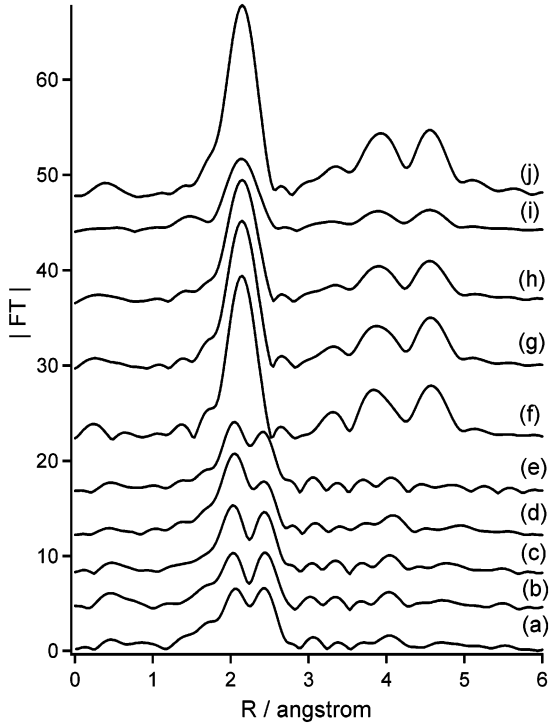

Figure 7. Fourier transforms of Ni K-edge k^3-weighted EXAFS of Pd−Ni/SiO_2, Ni/SiO_2, and Ni foil: (a, b, c, d, and e) Pd−Ni/SiO_2 with deposited carbons of C/(Pd + Ni) = 0 (fresh), 7, 310, 860, and 2360, respectively; (f, g, h, and i) Ni/SiO_2 with deposited carbons of C/Ni = 0 (fresh), 50, 650, and 1100, respectively; (j) Ni foil. Intensity of |FT| for a Ni foil was decreased to one-third.

Figure 6 shows Ni K-edge k^3-weighted EXAFS of Pd−Ni/SiO_2 and Ni/SiO_2, before and after methane decomposition, and of Ni foil. Fourier transforms of these EXAFS spectra in Figure 6 (RSF, radial structure function) were shown in Figure 7. The pattern of k^3-weighted EXAFS oscillation of fresh Ni/SiO_2 (spectrum f) was similar to that of Ni foil (spectrum j), although the intensity of oscillation was different between them. The pattern and intensity of EXAFS oscillation for Ni/SiO_2 did not change significantly in the C/Ni range from 0 to 650 (spectra f−h), where the activity of the catalyst for methane decomposition was kept high. These results indicate that Ni species in Ni/SiO_2 were always present as Ni metal and the local structure and crystallite size of the metal did not change appreciably when the catalyst decomposed methane actively. However, the intensity of EXAFS oscillation became weak at the deactivation stage of Ni/SiO_2 (spectrum i), although the oscillation pattern for the deactivated catalyst was similar to that for the fresh one. XANES spectra of Ni/SiO_2 suggested the formation of Ni carbide species at the deactivation stage. Thus, the change of the EXAFS spectrum at the deactivation of Ni/SiO_2 would be assignable to the formation of Ni carbide species.

Ni K-edge k^3-weighted EXAFS of fresh Pd−Ni/SiO_2 was different from that of Ni foil, suggesting the formation of Pd−Ni alloys in the catalyst. The intensity and pattern of all the EXAFS spectra for Pd−Ni/SiO_2 were similar to each other, irrespective of different amounts of deposited carbons, suggesting that the local structure around Ni atoms in Pd−Ni alloys did not change appreciably during methane decomposition.

The structural change of metal components during methane decomposition was furthermore clarified by Fourier transforms of EXAFS (RSFs) in Figure 7. A peak due to the Ni−Ni bond was observed in the range of 1.8−2.5 Å for all the RSFs of Ni/SiO_2, and the peak was located at the same position as that for Ni foil. The peak due to Ni−Ni bond for deactivated Ni/SiO_2 was weaker and broader compared to that for the fresh catalyst, while the intensity and width of the peak were unchanged in the C/Ni range ≤650. The spectral change at the deactivation stage of Ni/SiO_2 would be assignable to the formation of Ni carbide species, as will be described below in detail based on the structural parameters for Ni species estimated by curve-fitting of EXAFS.

RSF for fresh Pd−Ni/SiO_2 showed two peaks at 2.1 and 2.4 Å. These peaks could be assigned to Ni−Ni and Ni−Pd bonds in Pd−Ni alloys based on the results described earlier. The relative intensity of two peaks for Pd−Ni/SiO_2 catalysts did not change significantly during methane decomposition. These results implied that the fraction of each metal in Pd−Ni alloys and the crystallite size of the alloys were unchanged during the reaction.

Figure 8 shows Pd K-edge k^3-weighted EXAFS spectra of Pd/SiO_2 and Pd−Ni/SiO_2, before and after methane decomposition, and of Pd foil. Fourier transforms (RSFs) of EXAFS in Figure 8 were depicted in Figure 9. The pattern of EXAFS oscillation for fresh Pd/SiO_2 (spectrum f) was consistent with that for Pd foil, although the intensity of oscillation for the catalyst was weaker than that for Pd foil. Thus, Pd species in fresh Pd/SiO_2 were present as Pd metal. Contact of methane with Pd/SiO_2 to C/Pd = 7 (spectrum g) resulted in the decrease of intensity as well as the change of the peak position for the EXAFS oscillation, while appreciable change of the spectra for the catalyst was not observed in the range of C/Pd ≥ 7. RSFs of Pd/SiO_2 in Figure 9 also implied the structural change of Pd metal after contact with methane. The peak at 2.4 Å due to the Pd−Pd bond in fresh Pd/SiO_2 became smaller and broader after deposition of carbons to C/Pd ≥ 7.

Pd K-edge k^3-weighted EXAFS spectrum of fresh Pd−Ni/SiO_2 (spectrum a) in Figure 8 suggested that Pd species in the

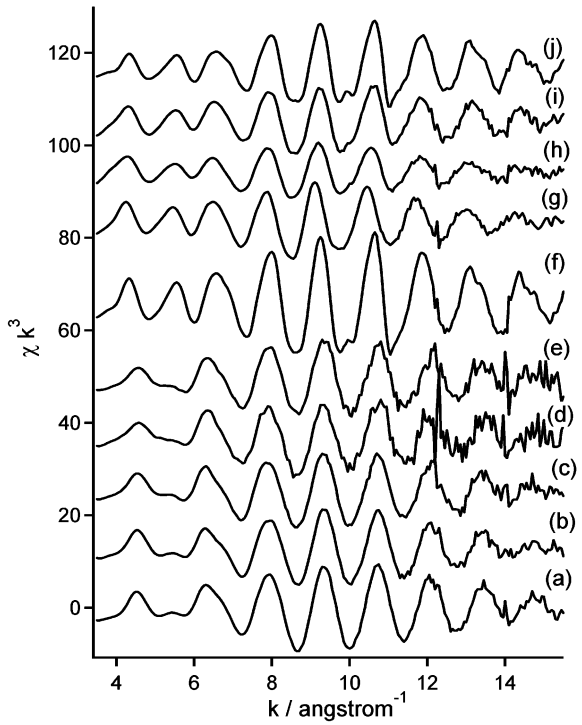

Figure 8. Pd K-edge k^3-weighted EXAFS of Pd/SiO_2, $Pd-Ni/SiO_2$, and Pd foil: (a, b, c, d, and e) $Pd-Ni/SiO_2$ with deposited carbons of C/(Pd + Ni) = 0 (fresh), 7, 310, 860, and 2360, respectively; (f, g, h, and i) Pd/SiO_2 with deposited carbons of C/Pd = 0 (fresh), 7, 118, and 260, respectively; (j) Pd foil. Intensity of χk^3 for a Pd foil was decreased to one-third.

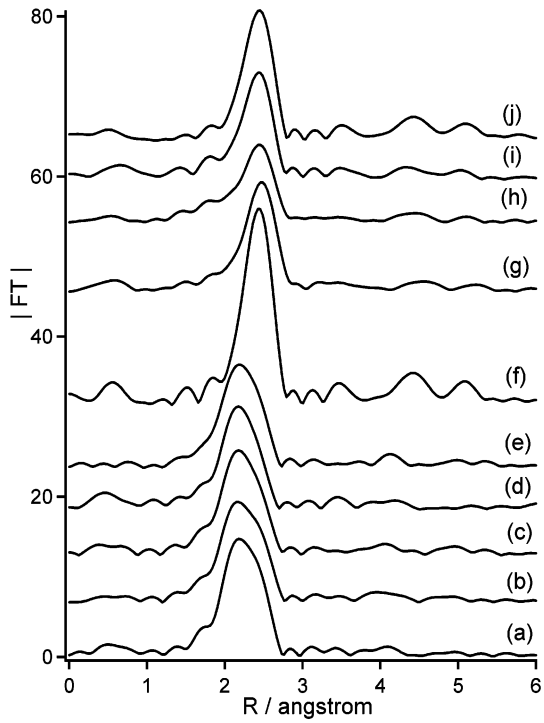

Figure 9. Fourier transforms of Pd K-edge k^3-weighted EXAFS of Pd/SiO_2, $Pd-Ni/SiO_2$, and Pd foil: (a, b, c, d, and e) $Pd-Ni/SiO_2$ with deposited carbons of C/(Pd + Ni) = 0 (fresh), 7, 310, 860, and 2360, respectively; (f, g, h, and i) Pd/SiO_2 with deposited carbons of C/Pd = 0 (fresh), 7, 118, and 260, respectively; (j) Pd foil. Intensity of |FT| for a Pd foil was decreased to one-third.

catalyst were not Pd metal but Pd−Ni alloys, since the spectrum of the catalyst was significantly different from that of Pd foil. The pattern and intensity of EXAFS oscillations for all $Pd-Ni/SiO_2$ (spectra a−e) were similar to each other regardless of different amounts of deposited carbons. A peak in the RSF of fresh $Pd-Ni/SiO_2$ in Figure 9 was positioned at 2.1 Å, while a peak due to the Pd−Pd bond appeared at 2.4 Å in the RSF of Pd foil. In addition, a shoulder peak was observed at 2.4 Å for the RSFs of $Pd-Ni/SiO_2$ catalyst. The peak in the range of 1.8−2.8 Å for $Pd-Ni/SiO_2$ would correspond to Pd−Ni and Pd−Pd bonds in Pd−Ni alloys on the basis of the results described earlier. Appreciable changes of the RSFs for $Pd-Ni/SiO_2$ were not observed during methane decomposition. Thus, the local structure around Pd atoms in Pd−Ni alloys did not change during the reaction.

TABLE 1: Structural Parameters Estimated by Curve-Fitting[e] for Ni K-edge EXAFS of Ni/SiO_2 and $Pd-Ni/SiO_2$

catalyst	C/M[a]	shell	CN[b]	*R*/Å[c]	σ/Å[d]
Ni/SiO_2	0	Ni−Ni	7.5 ± 0.7	2.48	0.062
Ni/SiO_2	49	Ni−Ni	8.1 ± 0.6	2.48	0.066
Ni/SiO_2	650	Ni−Ni	6.2 ± 0.5	2.48	0.067
Ni/SiO_2	1100	Ni−Ni	4.6 ± 0.5	2.48	0.070
		Ni−Ni	2.4 ± 0.6	2.67	0.120
$Pd-Ni/SiO_2$	0	Ni−Ni	3.5 ± 0.3	2.55	0.096
		Ni−Pd	3.6 ± 0.2	2.59	0.079
$Pd-Ni/SiO_2$	7	Ni−Ni	5.2 ± 0.5	2.58	0.106
		Ni−Pd	4.0 ± 0.3	2.59	0.082
$Pd-Ni/SiO_2$	310	Ni−Ni	4.1 ± 0.5	2.57	0.093
		Ni−Pd	4.3 ± 0.3	2.58	0.079
$Pd-Ni/SiO_2$	860	Ni−Ni	4.4 ± 0.4	2.55	0.099
		Ni−Pd	4.1 ± 0.3	2.58	0.080
$Pd-Ni/SiO_2$	2360	Ni−Ni	3.9 ± 0.5	2.54	0.088
		Ni−Pd	4.2 ± 0.4	2.57	0.081

[a] Carbon yield [C/Ni or C/(Pd + Ni)]. [b] Coordination number. [c] Interatomic distance. [d] Debye−Waller factor. [e] Inversely Fourier transformed data for Fourier peak in the *R* range of 1.5−2.7 Å were analyzed by a curve−fitting methods.

Furthermore, curve-fitting analyses for the EXAFS in Figures 6−9 were performed in order to clarify the local structures around Pd and Ni atoms in Ni/SiO_2, Pd/SiO_2, and $Pd-Ni/SiO_2$ during methane decomposition. The structural parameters evaluated by curve-fitting of Ni K-edge EXAFS were listed in Table 1. The coordination number and interatomic distance of the Ni−Ni bond in fresh Ni/SiO_2 (Table 1) were evaluated to be 7.5 and 2.48 Å, respectively. The interatomic distance and coordination number of the Ni−Ni bond in Ni/SiO_2 were kept to almost the same values in the C/Ni range from 0 to 650, where the catalyst showed high activity for methane decomposition. However, at the deactivation stage of Ni/SiO_2, another Ni−Ni bond of longer interatomic distance (2.67 Å) was formed in addition to the Ni−Ni bond of the same distance as that of the fresh catalyst. XANES spectra of Ni/SiO_2 suggested the formation of Ni carbide species at the deactivation stage. Because the feature of EXAFS oscillation for the deactivated Ni/SiO_2 was similar to that for Ni foil of face-centered cubic structure (fcc), the Ni species in deactivated Ni/SiO_2 would be of fcc structure. It is well-accepted that carbon atoms are introduced in the vacancy (octahedral and tetrahedral pockets) in Ni metal of fcc structure, when carbon atoms diffuse in the metal.[16,18] The radius of carbon atoms is larger than that of the vacancy in Ni metal. Thus, the dissolution of carbon atoms in Ni metal should elongate the interatomic distance of the Ni−Ni bond in Ni metal. XANES and EXAFS spectra suggested that the local structure of Ni metal did not change when Ni/SiO_2 showed high activity for methane decomposition. It is likely that the concentration of carbons dissolved in Ni metal was low when Ni/SiO_2 decomposed methane actively. Even if the concentration of carbon atoms in Ni metal would be high

TABLE 2: Structural Parameters Estimated by Curve-Fitting[e] for Pd K-edge EXAFS of Pd/SiO_2 and $Pd-Ni/SiO_2$

catalyst	C/M[a]	shell	CN[b]	R/Å[c]	σ/Å[d]
Pd/SiO_2	0	Pd−Pd	7.8 ± 0.7	2.74	0.070
Pd/SiO_2	7	Pd−Pd	4.2 ± 0.4	2.73	0.067
		Pd−Pd	3.2 ± 0.3	2.82	0.069
Pd/SiO_2	118	Pd−Pd	4.5 ± 0.6	2.74	0.073
		Pd−Pd	1.8 ± 0.5	2.84	0.072
Pd/SiO_2	260	Pd−Pd	4.1 ± 0.3	2.73	0.059
		Pd−Pd	2.0 ± 0.3	2.82	0.057
$Pd-Ni/SiO_2$	0	Pd−Pd	3.5 ± 0.6	2.67	0.084
		Pd−Ni	3.6 ± 0.4	2.57	0.060
$Pd-Ni/SiO_2$	7	Pd−Pd	3.9 ± 0.6	2.67	0.085
		Pd−Ni	4.0 ± 0.6	2.57	0.069
$Pd-Ni/SiO_2$	310	Pd−Pd	3.0 ± 0.7	2.67	0.082
		Pd−Ni	4.1 ± 0.5	2.58	0.073
$Pd-Ni/SiO_2$	860	Pd−Pd	3.0 ± 0.7	2.66	0.096
		Pd−Ni	3.4 ± 0.5	2.57	0.057
$Pd-Ni/SiO_2$	2360	Pd−Pd	3.5 ± 0.7	2.67	0.087
		Pd−Ni	4.2 ± 0.5	2.57	0.071

[a] Carbon yield [C/Ni or C/(Pd + Ni)]. [b] Coordination number. [c] Interatomic distance. [d] Debye−Waller factor. [e] Inversely Fourier transformed data for Fourier peak in the R range of 1.5−2.7 Å were analyzed by a curve−fitting methods.

at the steady state of methane decomposition, carbons dissolved in the metal may be deposited from the metal when the catalyst was cooled to room temperature for the spectroscopic measurements. On the other hand, XANES and EXAFS showed the formation of Ni carbides at the deactivation of Ni/SiO_2. Thus, Ni carbides that were stable under the reaction conditions would be formed at the deactivation stage of Ni/SiO_2. The Ni carbides did not precipitate carbon atoms dissolved in them at the reaction conditions or at room temperature for the spectroscopic measurements.

The structural parameters estimated by curve-fitting for fresh $Pd-Ni/SiO_2$ showed the presence of Ni−Ni and Ni−Pd bonds, i.e., Pd−Ni alloys. The coordination number of the Ni−Ni bonds was similar to that of Ni−Pd bonds for the fresh catalyst. It should be noted that mole ratio Pd/(Pd + Ni) for $Pd-Ni/SiO_2$ was adjusted to be 0.5. Therefore, the coordination number estimated by curve-fitting suggests that Ni and Pd atoms were distributed uniformly in Pd−Ni alloys. The sum of the coordination numbers of Ni−Ni and Ni−Pd bonds for $Pd-Ni/SiO_2$ with deposited carbons of C/(Pd + Ni) = 7 was slightly larger compared to that for the fresh catalyst. Ni K-edge XANES spectra of $Pd-Ni/SiO_2$ suggested that a part of Ni species was reduced into the metallic state at a very early stage of the reaction. The coordination numbers of Ni−Ni and Ni−Pd bonds would become larger by contact of methane with the fresh $Pd-Ni/SiO_2$, because the reduction of Ni species enhanced the formation of Pd−Ni alloys. In addition, the shape of Pd−Ni alloy particles changed at very early stage of the reaction, as will be described later. In general, the coordination number of metal−metal bonds becomes greater as the crystallite size of the metal increases. The change of shape of Pd−Ni alloys at very early stage of the reaction may be accompanied with an increase of crystallite size of Pd−Ni alloys. In contrast, the coordination number of Ni−Ni and Ni−Pd bonds for $Pd-Ni/SiO_2$ was unchanged appreciably in the range of C/(Pd + Ni) ≥ 7. Therefore, the local structure around Ni atoms in Pd−Ni alloys and the crystallite size of the alloys did not change significantly during methane decomposition.

The structural parameters evaluated by curve-fitting for Pd K-edge EXAFS of Pd/SiO_2 and $Pd-Ni/SiO_2$ were listed in Table 2. The interatomic distance of Pd−Pd bond for fresh Pd/SiO_2 was evaluated to be 2.74 Å, which was the same distance as that in Pd foil. After contact of methane with Pd/SiO_2 catalyst, a Pd−Pd bond with longer interatomic distance (2.82−2.84 Å) than that of Pd metal was observed in addition to a Pd−Pd bond of the same distance as that for Pd foil. It was reported that Pd carbides were formed by contact of hydrocarbons with Pd metal.[27] The interatomic distance of Pd−Pd bonds in Pd carbides, which was evaluated by curve-fitting of EXAFS, was reported to be 2.81 Å. This value was similar to that in the present study (2.82−2.84 Å). Thus, appearance of Pd−Pd bonds with longer interatomic distance could be assignable to the formation of Pd carbides in Pd/SiO_2 during methane decomposition. It should be noted that the sum of the coordination numbers of the two kinds of Pd−Pd bonds decreased slightly with the amount of deposited carbons. This result implied that the crystallite size of Pd metal and/or Pd carbides became smaller gradually as methane decomposition proceeded on Pd/SiO_2 catalyst. In fact, TEM images of Pd/SiO_2 after methane decomposition showed the fragmentation of Pd particles into smaller ones, as will be described later.

The curve-fitting results for fresh $Pd-Ni/SiO_2$ suggested the presence of Pd−Ni alloys. The coordination number of Pd−Pd bonds for fresh $Pd-Ni/SiO_2$ was almost the same as that of Pd−Ni bonds, suggesting that each component (Pd and Ni) was distributed in Pd−Ni alloys uniformly. Significant change in the coordination numbers of Pd−Pd and Pd−Ni bonds was not observed during methane decomposition. Thus, the local structure around Pd atoms in Pd−Ni alloys and the crystallite size of the alloys did not change appreciably during methane decomposition over $Pd-Ni/SiO_2$. In addition, the formation of Pd−Pd, Ni−Ni, or Pd−Ni bonds with interatomic distances longer than those in fresh $Pd-Ni/SiO_2$ could not be found during methane decomposition from Tables 1 and 2, while Pd−Pd or Ni−Ni bonds with longer interatomic distance, which were assignable to the formation of Pd or Ni carbides, were observed in the case of Pd/SiO_2 or Ni/SiO_2. These results suggest that Pd−Ni alloys were not transformed into metal carbides during methane decomposition. It is likely that $Pd-Ni/SiO_2$ showed the longer catalytic life for methane decomposition because Pd−Ni alloys did not change into stable metal carbides under the reaction conditions.

Shape of Catalytically Active Metal Components in the Catalysts. Figure 10 shows TEM images of carbon nanofibers deposited on Ni/SiO_2 and Pd/SiO_2 by methane decomposition. It was found that carbons deposited from methane grew with a filamentous structure in TEM image a for Ni/SiO_2. A Ni metal particle was always present at the tip of carbon nanofiber, as shown in TEM images a and b. In the case of Pd/SiO_2, similar carbon nanofibers to those on Ni/SiO_2 were observed in TEM images c and d, i.e., a Pd particle was present at the tip of carbon nanofiber. The following mechanism is generally accepted for the growth of carbon nanofibers through methane decomposition over supported Ni and Pd catalysts.[4,9,28] Methane is decomposed on the (100) and (110) facets of the metal surface into hydrogen and carbon atoms with a simultaneous evolution of molecular hydrogen. The carbon atoms on the metal surface diffuse to the other side of the metal particle through the surface or the bulk, precipitating them as graphite layers on the (111) facets of the metal. The building of graphite layers would grow carbon nanofibers that were composed of the stacked cones of curved basal planes, i.e., fish-bone-type carbon nanofibers. The decomposition of methane must proceed steadily when there is a balance among the decomposition rate of methane into carbon and hydrogen atoms on one side of a metal particle, the rate of

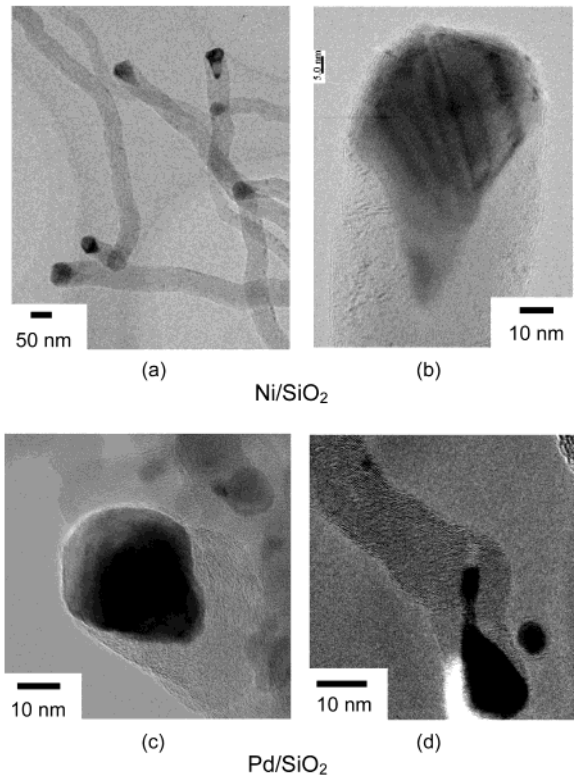

Figure 10. TEM images of carbon nanofibers deposited on Ni/SiO_2 (a and b) and Pd/SiO_2 (c and d).

diffusion of carbon atoms, and the rate of graphitization of carbon atoms at the other side of the metal particle. The deactivation of the catalysts would result from imbalance among these rates, which brought about the formation of metal carbides stable at the reaction conditions. The metal carbides could not precipitate carbon atoms. The formation of metal carbides at the deactivation stage of Ni/SiO_2 and Pd/SiO_2 was observed by XANES and EXAFS as described earlier. The imbalance among these rates may result from the coating of the active metal surface for methane decomposition with deposited carbon layers. In addition, it is worthwhile noting that a tail of the Pd particle present at the tip of carbon nanofiber was elongated in the direction of fiber axis, while the elongation of Ni metal particles was not observed during methane decomposition over Ni/SiO_2. The elongated Pd particle seems to be liable to be fragmented into two particles. Because the fragmented Pd metal was left in the interior of carbon nanofiber, it could not catalyze methane decomposition. The curve-fitting results for Pd K-edge EXAFS of Pd/SiO_2 suggested that the coordination number of Pd−Pd bonds decreased gradually during methane decomposition. The decrease of coordination number of Pd−Pd bonds could be assignable to the fragmentation of Pd metal and/or Pd carbide at the tip of fibers into smaller ones. The fragmentation of Pd particles would be also one of the reasons why Pd/SiO_2 catalyst was deactivated for methane decomposition.

Figure 11 shows TEM images of $Pd-Ni/SiO_2$ catalyst before and after the methane decomposition. Many darker spots were observed in TEM images of fresh $Pd-Ni/SiO_2$ (a and b). Energy dispersive spectra (EDS) for some of the darker spots were measured at the same time as the TEM images. The results of EDS showed that the darker spots were composed of Pd and Ni atoms, and the mole ratio of Pd/(Pd + Ni) was estimated to be ca. 0.5. These results are consistent with the conclusion drawn by the curve-fitting for EXAFS of $Pd-Ni/SiO_2$, that is, Pd and Ni atoms were distributed uniformly in Pd−Ni alloy particles.

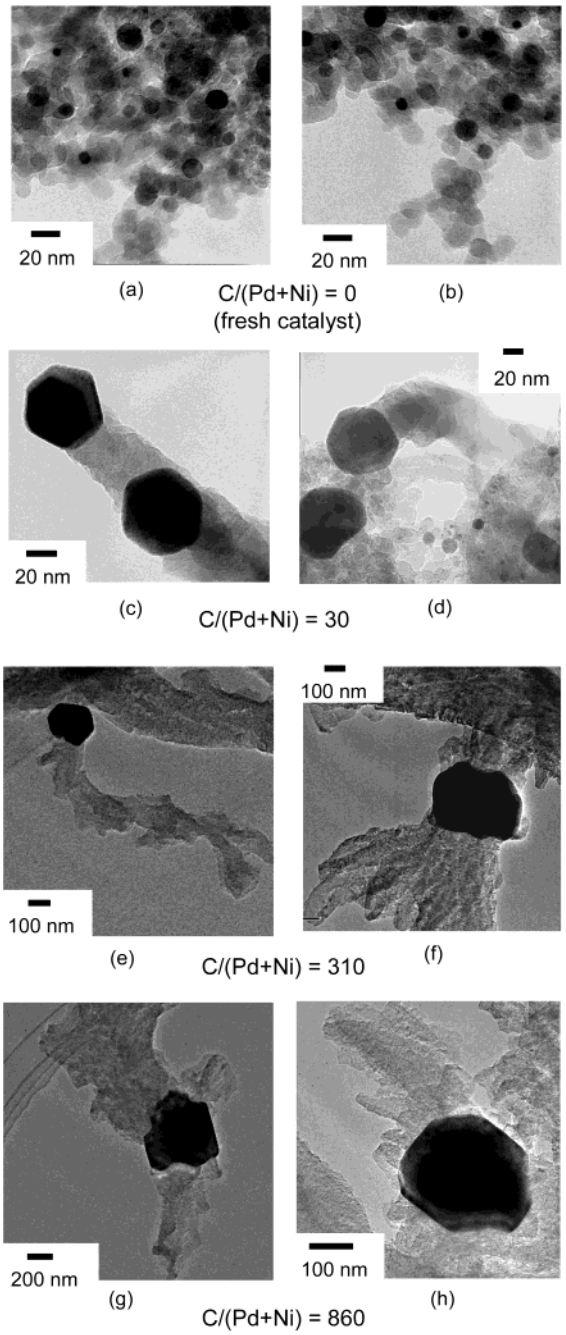

Figure 11. TEM images of $Pd-Ni/SiO_2$ catalyst before and after the methane decomposition.

TEM images a and b for the fresh $Pd-Ni/SiO_2$ showed that Pd−Ni alloy particles were not faceted. The shape of the alloy particles was changed by contact of methane. As shown in TEM images c and d of the catalyst with C/(Pd + Ni) = 30, most of Pd−Ni alloy particles were well-faceted, i.e., of hexagon in shape, and carbon nanofibers grew from a facet of well-faceted particle. The layers of graphite in the fibers were stacked in parallel to the facet to deposit carbon atoms and in perpendicular to the fiber axis, although the graphitization degree of the fibers seemed to be poor in the TEM images. The shape of Pd−Ni alloys changed gradually as methane decomposition proceeded over $Pd-Ni/SiO_2$ catalyst. TEM images e and f for $Pd-Ni/SiO_2$ catalyst with C/(Pd + Ni) = 310 showed that Pd−Ni alloy particles are facetted into polyhedrons. It should be noted that carbons were precipitated from several facets of a Pd−Ni alloy particle in the range of C/(Pd + Ni) ≥ 310 to form branched or assembled carbon nanofibers. When larger amounts of carbons

were deposited on Pd−Ni/SiO_2 catalyst, the surface disorder of Pd−Ni alloy particles was accelerated and the alloy particles grew carbon fibers in many directions, while Ni metal particles in Ni/SiO_2 and Pd metal particles in Pd/SiO_2 grew carbon nanofibers in one direction. An increase in the number of facets to grow carbon nanofibers would decrease the concentration of carbon atoms dissolved in the alloys quickly, which prevented the formation of stable metal carbides. This must be one of the reasons why Pd−Ni/SiO_2 catalysts showed longer life for methane decomposition compared to that for Ni/SiO_2 and Pd/SiO_2. However, too great an increase of the number of facets to precipitate carbon atoms would decrease the number of the facets that decompose methane into hydrogen and carbon atoms. A decrease in the area of the facets to decompose methane must result in declination of the rate of methane decomposition and thus deactivate the catalytic activity of Pd−Ni/SiO_2.

Conclusion

We conclude as follows based on the results described earlier.

1. The local structure and crystallite size of Pd−Ni alloys in Pd−Ni/SiO_2 did not change significantly during methane decomposition, while Ni metal changed to Ni carbides at the deactivation stage of Ni/SiO_2 and Pd metal particles were fragmented into smaller ones during the reaction on Pd/SiO_2.

2. Carbon nanofibers grew from several facets in a Pd−Ni particle to form branched carbon nanofibers during methane decomposition over Pd−Ni/SiO_2, while Pd and Ni metal produced carbon nanofibers in one direction. The number of the facets to deposit carbon atoms in Pd−Ni alloys increased gradually as the methane decomposition proceeded over Pd−Ni/SiO_2.

References and Notes

(1) Muradov, N. Z. *Int. J. Hydrogen Energy* **1993**, *18*, 211.
(2) de Jong, K. P.; Geus, J. W. *Catal. Rev. Sci. Eng*. **2000**, *42*, 481.
(3) Otsuka, K.; Kobayashi, S.; Takenaka, S. *Appl. Catal. A Gen*. **2000**, *190*, 261.
(4) Baker, R. T. K. *Carbon* **1989**, *27*, 315.
(5) Ishihara, T.; Miyashita, Y.; Iseda, H.; Takita, Y. *Chem. Lett*. **1995**, 93.
(6) Aiello, R.; Fiscus, J. E.; zur Loye, H.-C.; Amiridis, M. D. *Appl. Catal. A Gen*. **2000**, *192*, 227.
(7) Choudhary, T. V.; Sivadinarayana, C.; Chusuei, C. C.; Klinghoffer, A.; Goodman, D. W. *J. Catal*. **2001**, *199*, 9.
(8) Takenaka, S.; Kobayashi, S.; Ogihara, H.; Otsuka, K. *J. Catal*. **2003**, *217*, 79.
(9) Rostrup-Nielsen, J. R. *Catalysis, Science and Technology*; Anderson, J. R., Boudart, M., Eds.; Springer: Berlin, 1984; Vol. 5.
(10) Sinfelt, J. H.; *Bimetallic catalysts: discoveries, concepts, and applications*; Wiley: New York, 1983.
(11) Toshima, N.; Yonezawa, T. *New J. Chem*. **1998**, 1179.
(12) Otsuka, K.; Seino, T.; Kobayashi, S.; Takenaka, S. *Chem. Lett*. **1999**, 1179.
(13) Bernardo, C. A.; Alstrup, I.; Rostrup-Nielsen, J. R. *J. Catal*. **1985**, *96*, 517.
(14) Teunissen, W.; de Groot, F. M. F.; Geus, J.; Stephan, O.; Tence, M.; Colliex, C. *J. Catal*. **2001**, *204*, 169.
(15) Bernardo, C. A.; Alstrup, I.; Rostrup-Nielsen, J. R. *J. Catal*. **1985**, *96*, 517.
(16) Alstrup, I. *J. Catal*. **1988**, *109*, 241.
(17) Kim, M. S.; Rodriguez, N. M.; Baker, R. T. K. *J. Catal*. **1991**, *131*, 60.
(18) Avdeeva, L. B.; Goncharova, O. V.; Kochubey, D. I.; Zaikovskii, V. I.; Plyasova, L. M.; Novgorodov, B. N.; Shaikhutdinov, Sh. K. *Appl. Catal. A* **1996**, *141*, 117.
(19) Reshetenko, T. V.; Avdeeva, L. B.; Ismagilov, Z. R.; Chuvilin, A. L.; Ushakov, V. A. *Appl. Catal. A Gen*. **2003**, *247*, 51.
(20) Takenaka, S.; Shigeta, Y.; Otsuka, K. *Chem. Lett*. **2003**, *32*, 26.
(21) Takenaka, S.; Shigeta, Y.; Tanabe, E.; Otsuka, K. *J. Catal*. **2003**, *220*, 468.
(22) Ankudinov, A.; Ravel, B.; Rehr, J. J.; Conradson, S. D. *Phys. Rev. B* **1998**, *58*, 7565.
(23) Takenaka, S.; Ogihara, H.; Otsuka, K. *J. Catal*. **2002**, *208*, 54.
(24) Yoshida, T.; Tanaka, T.; Yoshida, H.; Funabiki, T.; Yoshida, S. *J. Phys. Chem*. **1996**, *100*, 2302.
(25) Lu, P.; Teranishi, T.; Asakura, K.; Miyake, M.; Toshima, N. *J. Phys. Chem. B* **1999**, *103*, 9773.
(26) McCaulley, J. M. *J. Phys. Chem*. **1993**, *97*, 10372.
(27) McCaulley, J. M. *Phys. Rev. B* **1993**, *47*, 4873.
(28) Kępiński, L. *Catal. Today* **1999**, *50*, 237.